PHYSICAL REVIEW B VOLUME 7, NUMBER 5 1 MARCH 1973

Specific Heat of Two-Dimensional Heisenberg Antiferromagnets: K_2MnF_4 and K_2NiF_4 †

M. B. Salamon*
Department of Physics and Materials Research Laboratory, University of Illinois, Urbana, Illinois 61801

H. Ikeda
Institute for Solid State Physics, University of Tokyo Roppongi, Minato-ku, Tokyo, Japan
(Received 8 August 1972)

The specific heat capacities of the quasi-Heisenberg antiferromagnets K_2MnF_4 and K_2NiF_4 have been measured by means of ac calorimetric methods and, through a comparison with the isostructural compound K_2MgF_4, the magnetic contributions extracted. The magnetic components lie on a universal curve when plotted in units of $R\ln(2S+1)$ against the reduced temperature $T/T_c^{(2)}$, where $T_c^{(2)}$ is the respective ordering temperature. It is found that the entropy change of $R\ln(2S+1)$ is spread over the range $0.4 \leq T/T_c^{(2)} \leq 4$ with a peak in the specific heat at $\sim 1.5 T_c^{(2)}$. Smaller peaks are observed at the transition points and are attributed to the crossover to anisotropic behavior. Models for the two-dimensional Heisenberg magnet are discussed and a suggestion by Kuramoto is explored which produces good agreement with experiment and a transition temperature which is proportional to the critical exponent η.

I. INTRODUCTION

Interest in the problem of the two-dimensional Heisenberg ferromagnet and antiferromagnet has been spurred by several recent developments: (i) the rigorous proof by Mermin and Wagner[1] that no long-range order can exist above $T=0$ K; (ii) the suggestion,[2] based on series-expansion analysis, that the susceptibility (staggered for the antiferromagnet) diverges at the so-called Stanley–Kaplan temperature

$$T_c^{(2)} = J(z-1)[2S(S+1)-1]/5k_B \qquad (1)$$

for z neighbors of spin S coupled by the exchange energy J; (iii) clear evidence from neutron diffraction[3,4] that K_2MnF_4 and K_2NiF_4 have purely two-dimensional correlations above their Néel temperatures, but order abruptly in the third dimension below.

Numerous theoretical treatments of the two-dimensional Heisenberg model have sought to investigate further the physical properties of a system which behaves according to points (i) and (ii).[5–6] Since the simple random-phase-approximation (RPA) calculation[5] supports the result that no long-range order exists above absolute zero, efforts to date have centered on modifications of the RPA which lead to a divergent susceptibility at finite temperature. Lines[6] and Mubayi and Lange[7] achieve this end by using decoupling schemes in a Green's-function calculation which modify the power spectrum in such a way as to achieve complete short-range order without a concurrent appearance of long-range order. As we shall see, both methods lead to results which are quite different from experimental results on the prototype materials K_2MnF_4 and K_2NiF_4.

In view of the important role of the short-range correlations in the behavior of two-dimensional Heisenberg systems, we believe that knowledge of the behavior of the specific heat of the real Heisenberg-like systems will serve to guide the development of a theory for this class of magnetic materials. Accordingly, we have determined the specific heat capacities of the antiferromagnetic salts K_2MnF_4 and K_2NiF_4,[9] the two-dimensional properties of which have already been discussed extensively in the literature.[3,4] As a measure of the lattice contribution, we have also determined the specific heat capacity of the isostructural compound K_2MgF_4.

Our analysis shows that the three compounds have very nearly identical lattice specific heat capacities and that, after subtraction of the lattice component, the magnetic contribution from each salt can be scaled by the logarithm of the spin degeneracy and the Néel temperature into a universal curve which contains the entire spin entropy. Both salts show, in addition, a small peak at the Néel temperature which could be attributed to either the onset of Ising-like correlations or a change to three-dimensional ordering. We find that the anisotropy accounts well for the behavior of K_2MnF_4 but overestimates the width of the peak in K_2NiF_4.

Since earlier calculations do not agree with these results, we turn to a quite simple modification of the RPA scheme suggested recently by Kuramoto.[8] Using a more realistic expression for the wave-vector-dependent susceptibility, he finds that the transition temperature is proportional to the critical exponent η which measures the deviation from Ornstein–Zernike critical behavior.[10] We have ex-

tended this approach and find that such a calculation leads to quite satisfactory results for the short-range-order parameter and the specific heat.

II. EXPERIMENT

The specific heat capacity was measured as a function of temperature for each material using the ac calorimetric technique described previously.[11] Samples were cleaved from larger single crystals (usual thickness 0.15 mm), blackened on one side with "dag" graphite suspension, and cemented to 25-μ Chromel–Alumel thermocouples which had been flattened to 5 μ in the junction region.[12] Because of the poor thermal conductivity of these materials along the c axis (normal to the cleaved planes) care was taken to operate at a sufficiently low frequency ($f \lesssim 11$ Hz) to maintain the samples in internal thermal equilibrium.

Bulk crystals of K_2MnF_4 were prepared by one of us (H.I.) for use in neutron studies[4] using techniques described previously. Samples of K_2NiF_4 and K_2MgF_4 were obtained from a number of sources and all gave nearly identical results; the data presented here for K_2NiF_4 were taken on a sample prepared by Sakamoto. As no differences could be detected between cleaved and mechanically polished samples, we conclude that strains do not play an important role.

To calibrate the ac measurement it is necessary to have an absolute value for the specific heat capacity at some reference temperature. As no previous measurements have been reported for these materials, we have determined the heat capacities of the bulk crystals from which our samples were cleaved by means of the heat-pulse method. Manganin heaters were cemented to the small crystals (50 mg of K_2MnF_4 and 90 mg of K_2NiF_4) and the temperature rise detected with a thermocouple.

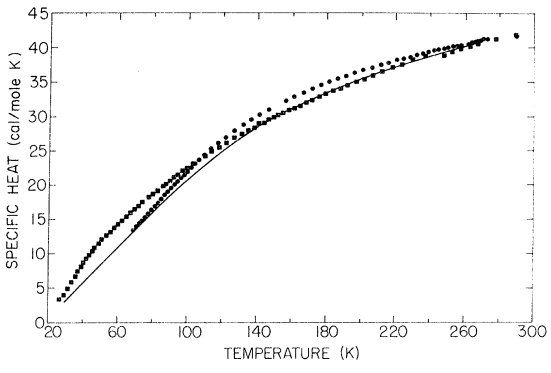

FIG. 1. Specific heat capacities of the planar compounds K_2MgF_4 (solid line), K_2MnF_4 (squares), and K_2NiF_4 (circles). The deviation of the data from the reference (solid line) is interpreted to arise from the magnetic contribution.

Measurements were performed at 295 K in the ac calorimeter by evacuating the sample space. Heat pulses of 10–100 mJ were applied, giving reproducible temperature rises of 100–1000 mK. Since measurements on such small samples are likely to be inaccurate, we calibrated the system with a sample of pure Cu, obtaining a specific heat capacity about 7% higher than accepted values, which we take as an indication of our systematic error.

Analysis of data taken by the ac method over a wide temperature range relies heavily on knowledge of the thermocouple sensitivity. Thermocouples used were from the same source and underwent identical mechanical and thermal treatment. The major error in our data lies in the assumption of standard sensitivity curves for our thermocouples, although in any case, the comparisons made here should remain valid.

III. RESULTS

The absolute specific heat capacities at room temperature were determined for the magnetic compounds with the results

$$C_p(29\ \mathrm{K})^{\mathrm{Mn}} = 43 \pm 1\ \mathrm{cal/mole\ K} \tag{2}$$

and

$$C_p(295\ \mathrm{K})^{\mathrm{Ni}} = 42 \pm 1\ \mathrm{cal/mole\ K}\ , \tag{3}$$

which are quite close to the Debye value of 42 cal/mole K. No absolute determination of the specific heat of K_2MgF_4 could be made as no large crystals were available. It should be kept in mind that values (2) and (3) are very likely overestimates of the actual specific heat capacities for bulk samples. For comparison purposes, we have taken the specific heat capacities to be equal at 295 K with the value

$$C_p(295\ \mathrm{K})^{\mathrm{av}} = 42.5\ \mathrm{cal/mole\ K}. \tag{4}$$

In the analysis below a slight adjustment in the room-temperature value of the K_2NiF_4 data, still within the range (3), was made to improve the fit to the universal curve.

The magnetic contribution to the specific heat is spread over a large range of temperature as may be seen in Fig. 1. There it may be noted that the data for K_2MnF_4 and the reference material are identical above 160 K which is $4T_c^{(2)}(\mathrm{Mn})$, where[4]

$$T_c^{(2)}(\mathrm{Mn}) = 42.1 \pm 0.1\ \mathrm{K}. \tag{5}$$

Similarly, the data for K_2NiF_4 rejoin the reference curve near 70 K, which is $0.7T_c^{(2)}(\mathrm{Ni})$, where[9]

$$T_c^{(2)}(\mathrm{Ni}) = 98.7 \pm 0.1\ \mathrm{K}. \tag{6}$$

We conclude that the magnetic contribution to the specific heat capacity is important in the range $0.7 \lesssim T/T_c^{(2)} \lesssim 4$.

Because of the similarity in magnetic struc-

ture,[3,4] we expect the magnetic specific heat capacities of K_2MnF_4 and K_2NiF_4 to behave similarly once account is taken of the differences in spin degeneracy and exchange constant. Accordingly, we have plotted the deviation of the specific heat capacity of each material from that of the reference material, scaled by $R\ln(2S+1)$, as a function of reduced temperature $T/T_c^{(2)}$ in Fig. 2. The spin on the Mn^{++} ion has been taken to be $\frac{5}{2}$, while that on the Ni^{++} ion, to be $S=1$ as determined in the spin-Hamiltonian calculation of Lines.[5] As mentioned above, it proved necessary to set the room-temperature specific heat of K_2NiF_4 to

$$C_p(295\ \mathrm{K})^{\mathrm{Ni}} = 42.8\ \mathrm{cal/mole\ K},$$

which is within the range of values determined in (3). At the maximum, the magnetic contribution is on the order of 10–20% of the total heat capacity of the samples. Therefore, the $\pm 0.5\%$ error for each curve is reflected in the rather large scatter of the points in this difference plot. Nonetheless, we argue that the points lie on a universal curve, the distinguishing features of which are (i) a peak of $\simeq 0.9R\ln(2S+1)$ at $1.5T_c^{(2)}$; (ii) a finite specific heat capacity of $\simeq 0.6R\ln(2S+1)$ at $T_c^{(2)}$; (iii) a tail which extends to $\sim 4T_c^{(2)}$; (iv) an entropy difference of $(0.95\pm 0.1)R\ln(2S+1)$ over the range $0.4 \le T/T_c^{(2)} \le 4$.

Because present theories are based on RPA techniques, they share some common faults. None of them predicts a spin dependence of the specific heat so that none produces an entropy change of $R\ln(2S+1)$. To compare these models with experiment, we have integrated the specific-heat curves to determine the entropy difference and considered the curve which results from dividing the specific heat by the entropy difference. The results are plotted in Fig. 2.

At one extreme, the RPA model[5] predicts no transition at finite temperatures, with a constant heat capacity of $1.5R$ near $T=0$ K. We have scaled the temperature to the large S limit of (1) for the quadratic layer structure

$$T_c^{(2)} = 1.2JS(S+1)/k_B \ . \qquad (7)$$

Without normalization the entropy change in the RPA model is $2.7R$, corresponding to a spin in excess of $S=6$.

At the other extreme, a Green's-function model due to Mubayi and Lange[7] predicts a divergence in the susceptibility at

$$T_c^{(2)} = 8JS(S+1)/3k_B \ , \qquad (8)$$

the molecular-field value. The low-temperature behavior of the specific heat was determined for this model for $S=\frac{1}{2}$ and is shown in Fig. 2 after division by $R\ln 2$. The qualitative agreement is good despite its overestimate of the size of the low-temperature heat capacity by a factor of 2 or more.

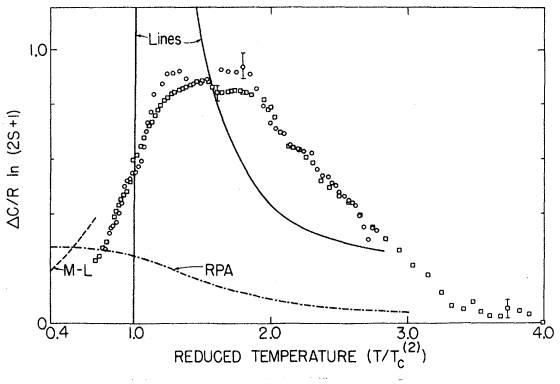

FIG. 2. Differences between the specific heat capacities of K_2MgF_4, the reference compound, and K_2MnF_4 (squares) and K_2NiF_4 (circles). The data are scaled by the expected entropy change $R\ln(2S+1)$ and are plotted as functions of the reduced temperature $T/T_c^{(2)}$, where $T_c^{(2)}$ values are given in Eqs. (5) and (6). The error bars represent only the noise contribution to scatter. Theoretical predictions from Ref. 6 (solid line), Ref. 7 (dashed line), and Ref. 5 (dot-dash line) are also scaled to the total entropy change for each curve.

The most complex of present models is due to Lines[6] and represents an improvement over earlier calculations as seen in Fig. 2. However, the peak in C_p above $T_c^{(2)}$ is far too large (approximately 4.8 on this scale) and occurs near $1.1T_c^{(2)}$, far closer than experiment indicates. Near $T_c^{(2)}$, the specific heat capacity increases linearly with $T-T_c^{(2)}$ which yields a critical exponent[9]

$$\alpha_{\mathrm{Lines}} = -1.$$

The same model predicts that the correlation length diverges with the critical exponent $\nu=1$, and thus violates the scaling law[10]

$$2\nu = 2-\alpha \ . \qquad (9)$$

This result seems to indicate that the cutoff procedure used in this model violates the scaling hypothesis despite the fact that the cutoff wavelength is proportional to the true correlation length.

In the vicinity of $T_c^{(2)}$ both K_2MnF_4 and K_2NiF_4 show a small peak in their specific heat capacities. These are shown in Fig. 3 as a function of reduced temperature to facilitate comparison of the curves. The peak in K_2MnF_4 is larger in amplitude and broader than that of K_2NiF_4. The temperatures of the peak values are

$$T_c^{(2)}(\mathrm{Mn}) = 42.1\pm 0.1\ \mathrm{K} \qquad (5)$$

and

$$T_c^{(2)}(\mathrm{Ni}) = 98.7\pm 0.1\ \mathrm{K} \qquad (6)$$

for K_2MnF_4 and K_2NiF_4, respectively, values which agree well with the transition to three-dimensional

long-range order observed by other methods.[3,4,13,14]

The origin of these small peaks in the specific heat capacities at the ordering temperature can be ascribed to two possible mechanisms: (i) close to $T_c^{(2)}$ the anisotropy energy becomes comparable to the energy in spin fluctuations, causing a cross over to behavior appropriate to an Ising system,[15] namely, a logarithmic divergence in the specific heat; (ii) near $T_c^{(2)}$ correlations within the plane become large enough to induce correlations between planes which then lead to the three-dimensional phase transition. Neutron-diffraction results in K_2NiF_4[3] show clearly that only the longitudinal susceptibility diverges, indicating that the phase transition is anisotropy dominated. No evidence of three-dimensional critical scattering was observed.

On the other hand, consideration of the size of the anisotropy in the two materials shows that there should be little difference in the behavior near $T_c^{(2)}$. In Table I, we have listed the anisotropy energy $g\mu_B H_A/k_B$ for each material[13,16] along with the nearest-neighbor exchange constant J. Transition temperatures calculated from (1) using these values of J are shown to be in excellent agreement with the temperature of the peak in C_p. Crossover[15] to Ising-like correlations should occur when $\epsilon = T/T_c^{(2)} - 1$ becomes comparable to

$$\Delta = g\mu_B H_A/kT_c^{(2)} \quad . \tag{10}$$

From Table I and Fig. 3, it is clear that the width of the peak in K_2NiF_4 is smaller than predicted on the basis of this argument. We note that the amplitude of the specific-heat peak ΔC scales with $\ln(2S+1)$ as expected.

Neutron diffraction measurements[3,4] indicate that the correlation length diverges with a critical exponent $\nu = 0.57 \pm 0.05$ for K_2NiF_4 and $\nu = 0.50 \pm 0.08$ for K_2MnF_4. Using these results in the scaling law (9) we conclude that

$$0.76 \leq \alpha \leq 1.16. \tag{11}$$

Owing to the extremely small amplitude of the peak, it is difficult to determine the critical exponent; for K_2NiF_4 it is impossible. For K_2MnF_4, using the baseline sketched in Fig. 3(a), we have plotted the deviation vs ϵ above the transition on the inset to Fig. 3(a). While the data are insufficient to give us any confidence in the critical exponent, it certainly seems to be reasonably close to (11).

TABLE I. Anisotropy and exchange constants for K_2MnF_4 and K_2NiF_4.

	$\frac{g\mu_B H_A}{k_B}$ (K)	$\frac{J}{k_B}$ (K)	$T_c^{(2)}$(calc) (K)	$T_c^{(2)}$(expt) (K)	Δ	$\frac{\Delta C}{R\ln(2S+1)}$
K_2NiF_4	1.1[a]	55[a]	99.0	98.7	0.01	0.052
K_2MnF_4	0.34[b]	4.1[b]	40.6	42.1	0.008	0.058

[a]Reference 5. [b]Reference 13.

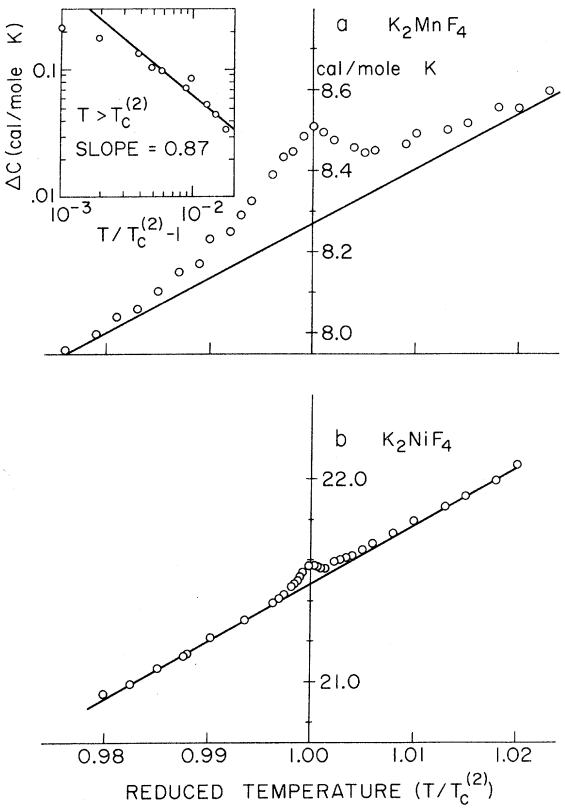

FIG. 3. Behavior of the specific heat capacity near $T_c^{(2)}$. (a) K_2MnF_4 data; inset shows the approximate power-law behavior above the transition assuming the baseline sketched in the figure and showing a critical exponent near 0.87. (b) K_2NiF_4 data; the peak is too small to permit even an estimate of the critical exponent.

IV. THEORY

A theory for the behavior of the two-dimensional Heisenberg model must lead to a finite temperature at which the susceptibility diverges, but no long-range order above absolute zero.[1,2] Since the RPA correctly predicts vanishing long-range order at finite temperatures, attention has centered on modifications which allow for a divergent susceptibility at the temperature $T_c^{(2)}$ [Eq. (1)] predicted by high-temperature series expansion. The problem can be discussed quite simply by considering the theorem

$$\tfrac{1}{3}NS(S+1) = k_B T \sum_{\vec{k}} \chi_{\vec{k}} \quad , \tag{12}$$

where χ_k is the Fourier transform of the longitudinal-spin correlation function which, in RPA,[5] is given by

$$\chi_{\vec{k}}^{RPA} = (2Jk^2 + \chi_0^{-1})^{-1} \quad , \tag{13}$$

where χ_0 is the static susceptibility. For three-di-

mensional lattices, the sum in (12) is well-behaved and leads to a finite temperature at which $\chi_0^{-1} \to 0$. In two dimensions, however, (12) becomes (approximating the zone by a circle of radius π/a)

$$\tfrac{1}{3}S(S+1) \cong \left(\frac{k_B T}{2J}\right) \frac{1}{2\pi} \int_0^{\pi} \frac{k\,dk}{k^2 + (2J\chi_0)^{-1}} \quad , \tag{14}$$

where k is measured in units of the inverse of the lattice constant. Since the integral is divergent in the limit that χ_0^{-1} vanishes, the transition occurs at $T = 0$ K in contradiction with the series-expansion result.[2]

In a rather bold move to modify this result, Lines[6] proposed to cut off the integral at a wave vector k_c which is temperature dependent. Elementary substitution of the limit k_c into (14) leads to the conclusion that the integral will remain finite so long as

$$\lim_{\chi_0 \to \infty} (2J\chi_0 k_c^2) = \text{finite}. \tag{15}$$

Since in the RPA the true correlation length varies as $\chi_0^{1/2}$, it was necessary to define the new length k_c^{-1} to be some fraction of the actual correlation length. While this is reasonable, the sharp cutoff implied has no physical basis and the theory, as we have seen, leads to results which are quite different than the observed behavior for quasi-Heisenberg systems.

Quite recently, Kuramoto[8] pointed out that a more realistic expression for $\chi_{\vec{k}}$ will lead to finite $T_c^{(2)}$ within the framework of the usual RPA method. We have extended this idea and find that it predicts behavior of the short-range correlation function and the specific heat which is quite similar to experimental results. The parameters which lead to a value of $T_c^{(2)}$ in agreement with (1) also seem to be reasonable choices in the light of both Ising-model results and experimental values.

We proceed by choosing the Fisher–Burford[17] (FB) approximant for $\chi_{\vec{k}}$:

$$\chi_{\vec{k}}^{\mathrm{FB}} \cong \frac{1}{2J} \frac{(\kappa^2 + \varphi^2 k^2)^{\eta/2}}{(\kappa^2 + k^2)} \quad , \tag{16}$$

where κ^{-1} is the correlation length and we have assumed that the parameters φ and η are small. At the critical point where κ vanishes, (12) becomes equal to

$$\tfrac{1}{3}S(S+1) \cong \frac{k_B T_c^{(2)}}{2J} \frac{\varphi^{\eta}}{2\pi} \int_0^{\pi} \frac{dk}{k^{1-\eta}} \quad , \tag{17}$$

which can be evaluated analytically. Thus, in the approximation of a Brillouin zone of radius π/a, we find that

$$T_c^{(2)} = \frac{4\eta J S(S+1)\pi^{1-\eta}}{3k_B \varphi^{\eta}} \quad . \tag{18}$$

This result supports the observation made by Kuramoto that a finite and positive value of η leads to the Stanley–Kaplan transition. Similar conclusions have been reached for the spherical model with an interaction having an $r^{-(d+2-\eta)}$ dependence,[18] and for the ideal Bose gas in two dimensions[19] with an energy dispersion relation of the form $k^{2-\eta}$. In all of these cases, it is the presence of a power less than 2 in the dispersion relation which leads to a nonvanishing transition temperature.

Substituting (16) into (12), assuming φ and η are constants, we obtain the temperature dependence of the correlation wave vector which we may then use to evaluate the related integral for the short-range-order parameter[5,6]

$$\frac{\langle \vec{S}_0 \cdot \vec{S}_a \rangle}{S(S+1)} = \frac{3k_B T}{S(S+1)} \frac{1}{(2\pi)^2} \int_{\text{zone}} d\vec{k} \cos(\vec{k} \cdot \vec{a})\, \chi_{\vec{k}}^{\mathrm{FB}} \tag{19}$$

to find the nearest-neighbor correlation function $\langle \vec{S}_0 \cdot \vec{S}_a \rangle$. As above, we approximate the zone by a circle of radius π/a and find that

$$\frac{\langle \vec{S}_0 \cdot \vec{S}_a \rangle}{S(S+1)} = \frac{3k_B T}{2\pi S(S+1)} \int_0^{\pi} dk\, k J_0(k)\, \chi_{\vec{k}}^{\mathrm{FB}} \quad , \tag{19'}$$

where $J_0(k)$ is a Bessel function of zero order. This approximation introduces errors into our results as does the use of k^2 in the FB approximant (16) rather than a function $K(k)$ which reflects the lattice structure. We have used the present approximations in the interest of obtaining the transition temperature (18) in closed form.

In Fig. 4 we have plotted the results for the nearest-neighbor correlation function calculated in this approximation for two values of η holding φ constant. As η is reduced, the transition temperature decreases as shown by (18) and the value of the correlation function at $T_c^{(2)}$ increases. In the limit $\eta \to 0$, we return to the RPA result with $T_c^{(2)} = 0$ K and with $\langle \vec{S}_0 \cdot \vec{S}_a \rangle$ reaching $S(S+1)$. In the present approximation the temperature scale is expanded considerably over that of Lines,[6] owing again to our use of k^2 rather than $2 - \cos k_x a - \cos k_y a$. The values $\eta = 0.25$ and $\varphi = 0.03$ are appropriate to the two-dimensional Ising model.[17]

Since the transition temperature is known from series expansion, we may choose values of η and φ which agree with (1). Taking the large-S limit of (1) given by (7) and comparing it with (18), we find that

$$4\eta\pi^{1-\eta}/3\varphi^{\eta} = 1.2 \tag{20}$$

leads to the same transition temperature for the two calculations. In Fig. 5, we have plotted curves for the derivative of the nearest-neighbor correlation function with respect to temperature for several values of the parameters which satisfy (20).

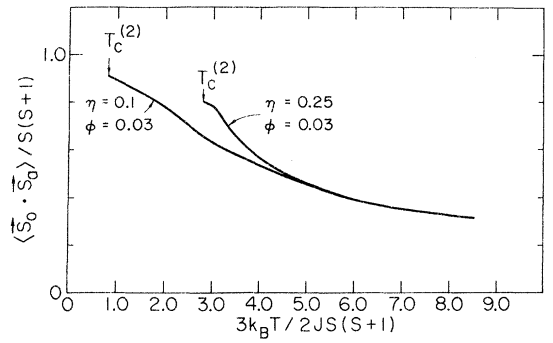

FIG. 4. Nearest-neighbor correlation function calculated from the Fisher–Burford approximant to the wave-vector-dependent susceptibility for two different values of η and with $\varphi = 0.03$.

The choice

$$\eta = 0.19, \quad \varphi = 0.03 \tag{21}$$

appears to be favorable since the peak in the derivative is close to the peak in the observed specific heat and the value at $T_c^{(2)}$ is approximately the same fraction of the peak value found experimentally. Further, this value of η is close to that determined from neutron-diffraction data[3,4] away from $T_c^{(2)}$ and φ is appropriate to the two-dimensional Ising model.

The result for the short-range correlation function $\langle \vec{S}_0 \cdot \vec{S}_a \rangle$ for values (21) is shown in Fig. 6. At $T_c^{(2)}$, $\langle \vec{S}_0 \cdot \vec{S}_a \rangle$ reaches 84% of its maximum possible value; this is approximately the maximum spin projection possible even at absolute zero owing to zero-point motion.[5] Also shown in Fig. 6 is an estimate of the short-range-order parameter for K_2NiF_4 determined from an analysis of the F^{19} nuclear resonance[20] and the prediction of Lines's theory. The analysis of the NMR data assumes the divergence of the exchange frequency ω_e at $T_c^{(2)}$ manifested by the increasing NMR linewidth of F^{19} nuclei having only one Ni neighbor. The presence of thermodynamic slowing down would reduce both ω_e and the size of the short-range-order parameter near $T_c^{(2)}$. The present calculation is clearly an improvement over the Lines model, and could be improved further by forcing the dispersion curve to approach the zone boundary with zero slope, thus compressing the temperature scale somewhat. We note that there is some inconsistency between the NMR data and the specific-heat results, since the NMR data indicate that the maximum slope of $\langle \vec{S}_0 \cdot \vec{S}_a \rangle$ (peak in C_p) occurs above $2T_c^{(2)}$.

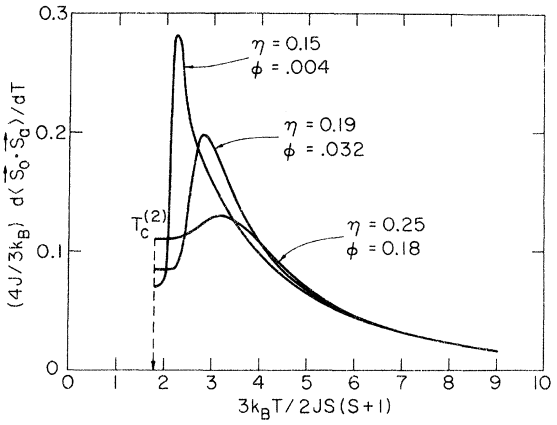

FIG. 5. Temperature derivative of the nearest-neighbor correlation function using the Fisher–Burford approximant. Values of η and φ were chosen to produce a critical temperature which agrees with the prediction of series-expansion analysis.

The specific heat capacity is related to the derivatives of the nearest-neighbor correlation function shown in Fig. 5 through the expression

$$C_{H=0} = \tfrac{1}{2}NzJ\left(\frac{d\langle \vec{S}_0 \cdot \vec{S}_a \rangle}{dT}\right)_{H=0} . \tag{22}$$

As with previous calculations, the specific heat determined in this way is spin-independent and must be normalized to the entropy change before comparison with experiment. In the present case, however, the specific heat is finite at the transition, leaving an unknown fraction of the total entropy change below $T_c^{(2)}$. For the parameters (21) 16% of the magnetic energy density has been acquired below $T_c^{(2)}$, as can be seen in Fig. 6, indicating that a similar fraction of the total entropy change also occurs below the transition. Therefore, we take the entropy change calculated from the specific-heat curve above the transition to be 84% of the total. The specific-heat curve calculated using the values (21) is plotted as a function of reduced temperature in units of the entropy change in Fig. 7 along with the experimental data from Fig. 2. The agreement is quite satisfactory in the in-

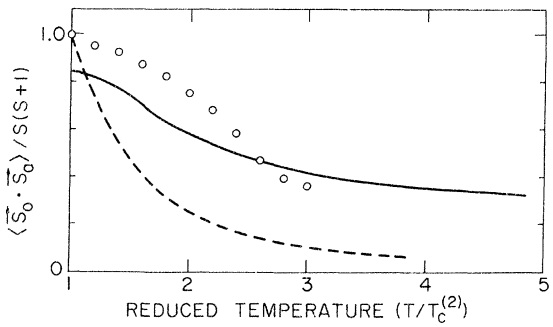

FIG. 6. Nearest-neighbor correlation function for the choice $\eta = 0.19$ and $\varphi = 0.03$ (solid line). Estimated experimental values (Ref. 20) are shown as circles and the prediction of Ref. 6 as a broken curve.

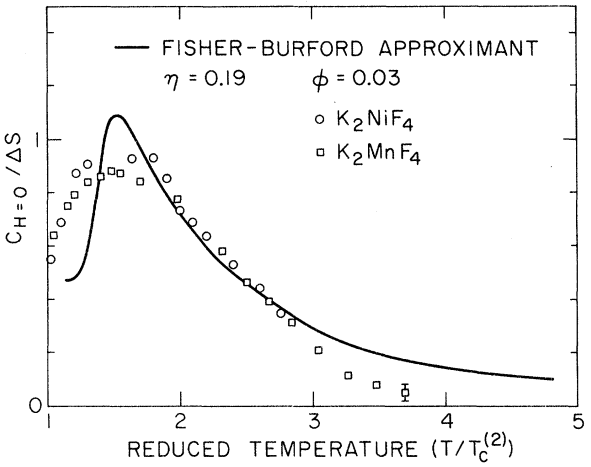

FIG. 7. Specific heat capacity calculated for $\eta = 0.19$ and $\varphi = 0.03$. Representative data from Fig. 2 are superimposed for comparison.

termediate temperature range, with a peak of approximately the correct size occurring at $1.5\ T_c^{(2)}$. The long tail on the calculated curve can be reduced by a more realistic behavior of $\chi_{\vec{k}}$ near the zone boundary. Using $2 - 2\cos k$ rather than k^2 in (16), for example, we obtain similar curves to those in Fig. 5, but with compression of the high-temperature portions of the curve by approximately 20%. The calculation does not satisfactorily predict the behavior near $T_c^{(2)}$, a feature noted in the analysis of neutron data[3] where η appears to change from 0.4 to ~0.2 in going from $T_c^{(2)}$ to $1.1\,T_c^{(2)}$.

Below $T_c^{(2)}$ there is no long-range order in the absence of anisotropy. This follows in the RPA from consideration of the integral equation which defines the long-range-order parameter $\bar{S}$,[8]

$$1 = \frac{2\bar{S}}{2\pi}\int_0^{\pi} dk\ k \coth\left(\frac{\bar{S}E(k)}{k_B T}\right) \quad . \tag{23}$$

Here $E(k)$ is the dispersion curve for excitations in the system. As noted above, when k is large compared with the correlation wave vector κ, the dispersion curve is no longer quadratic, the fact which leads to the Stanley–Kaplan transition in the present model. However, at low temperatures, we are clearly in the spin-wave regime where the dispersion relation is quadratic, and (23) requires that $\bar{S} = 0$ for all finite T. The presence of anisotropy modifies this result as has been discussed by Lines.[6]

We conclude that a satisfactory explanation of the properties of the two-dimensional Heisenberg magnet results if a more realistic form of the wave-vector-dependent susceptibility is appended to the theory. This approach is unsatisfactory in that it does not produce the transition in a natural way from the Hamiltonian and further, does not clearly display the physical interpretation of the parameter η.

V. DISCUSSION AND CONCLUSIONS

In a sense the present experiment is a negative result: there is no singularity of the specific heat at the ordering temperature $T_c^{(2)}$. Rather than disprove the occurrence of a Stanley–Kaplan transition in K_2MnF_4 and K_2NiF_4, this should be taken as additional evidence in its favor since the series-expansion results seem to indicate that there is no infinity in the specific heat.[21] In the usual sense, then, the Stanley–Kaplan transition is not second order. In fact, there is little to distinguish the behavior of the specific heat of the two-dimensional Heisenberg system from the one-dimensional Ising model, where there is no transition, except for the weak peak accompanying the crossover to anisotropic behavior. In view of the smooth behavior and the large temperature range involved, it seems likely that the high-temperature expansion would give a reasonable approximation to the actual behavior with a limited number of terms. We urge that such calculations be performed and compared with the universal curve we have extracted from our data in Fig. 2. Unlike the models discussed here, the series-expansion results should reflect the proper spin-dependence and would predict the true size and position of the peak in the specific heat.

We have extended the suggestion made by Kuramoto which places central importance on the critical parameter η in two dimensions. Of course, it is clear that, since η is defined through the long-range behavior of the correlation function, for $\kappa = 0$,

$$\langle S_0 S_R \rangle \sim R^{2-d-\eta} \quad , \tag{24}$$

where d is the dimensionality, if η is important at all, it is of most importance for $d = 2$. In the case of the two-dimensional Heisenberg model, Stanley and Kaplan[2] noted that even at low temperatures the correlation function (24) might decay with a small inverse power of R, a possibility which would account for the absence of true long-range order while the susceptibility, which is the sum of (24) over all R, continues to have a divergence. These observations would indicate that a model for the two-dimensional Heisenberg magnet should focus on the exponent η and include the possibility of a temperature dependence.

From an experimental point of view, we have been fortunate in the selection of K_2MgF_4 as a reference material, and in the fact that all three salts have very similar lattice specific heat capacities. No adjustments of the temperature scale

to reflect different effective Debye temperatures seem capable of producing the curve in Fig. 2, nor of giving an entropy change of $R\ln(2S+1)$ for each material. The ac method has been essential for the observation of the extremely small peaks at the ordering temperatures and the high resolution possible has facilitated the extraction of the broad magnetic contribution to the specific heat.

We conclude that thermodynamic measurements give further evidence that the ordering of the planar antiferromagnets K_2MnF_4 and K_2NiF_4 is of the Stanley–Kaplan type, with the anisotropy and three-dimensional nature of the ordered phase making only minor modifications in the over-all behavior.

Note added in proof. Yamada[22] has recently obtained similar results for the two-dimensional Heisenberg ferromagnet K_2CuF_4. The specific heat of that material does not fall on the curve of Fig. 7, but rather, resembles the curve of Fig. 5 with $\eta \cong 0.25$.

ACKNOWLEDGMENT

One of us (M. B. S.) wishes to acknowledge the hospitality of the Institute for Solid State Physics, University of Tokyo, where a portion of this research was performed while the author was a visiting scientist.

†Supported in part by the ARPA under Contract No. HC-15-67-C-0221 and by the National Science Foundation under Grant No. GH33750.

*Alfred P. Sloan Research Fellow.

[1]N. D. Mermin and H. Wagner, Phys. Rev. Letters 17, 1133 (1966).

[2]H. E. Stanley and T. A. Kaplan, Phys. Rev. Letters 17, 913 (1966).

[3]R. Birgeneau *et al.*, Phys. Rev. B 1, 2211 (1970); Phys. Rev. B 3, 1736 (1971).

[4]H. Ikeda and K. Hirakawa, J. Phys. Soc. Japan 33, 393 (1972); and (unpublished).

[5]M. E. Lines, Phys. Rev. 164, 736 (1967).

[6]M. E. Lines, Phys. Rev. B 3, 1749 (1971).

[7]V. Mubayi and R. V. Lange, Phys. Rev. 178, 882 (1969).

[8]Y. Kuramoto, Progr. Theoret. Phys. 46, 1293 (1971).

[9]M. B. Salamon and I. Hatta, Phys. Letters 36A, 85 (1971).

[10]L. P. Kadanoff *et al.*, Rev. Mod. Phys. 39, 395 (1967).

[11]M. B. Salamon, Phys. Rev. B 2, 214 (1970).

[12]P. R. Garnier, Ph.D. thesis (University of Illinois, 1972) (unpublished).

[13]D. J. Breed, Physica 37, 35 (1967).

[14]K. G. Srivastava, Phys. Letters 4, 55 (1963).

[15]M. Suzuki, Physics Letters 35A, 23 (1971).

[16]R. J. Birgeneau, F. DeRosa, and H. J. Guggenheim, Solid State Commun. 8, 13 (1970).

[17]M. E. Fisher and R. Burford, Phys. Rev. 156, 583 (1967).

[18]G. S. Joyce, Phys. Rev. 146, 349 (1966).

[19]J. D. Gunton and M. J. Buckingham, Phys. Rev. 166, 152 (1968).

[20]E. P. Maarshall, A. C. Botterman, S. Vega, and A. R. Miedema, Physica 41, 473 (1969).

[21]H. E. Stanley, Phys. Rev. Letters 20, 150 (1968).

[22]I. Yamada, J. Phys. Soc. Japan 33, 979 (1972).

PHYSICAL REVIEW B VOLUME 7, NUMBER 5 1 MARCH 1973

Magnetic Transitions in $CsNiCl_3$†

W. B. Yelon and D. E. Cox

Brookhaven National Laboratory, Upton, New York 11973

(Received 28 August 1972)

Recent NMR and specific-heat measurements have revealed the presence of magnetic phase transitions in $CsNiCl_3$ at 4.85 and 4.4 °K. Previous neutron-diffraction studies have revealed only one transition and we have, therefore reexamined a single crystal of $CsNiCl_3$ in the temperature range 1.6–5.0 °K by means of this technique. The use of neutrons of wavelength of 2.46 instead of 1.03Å gives improved resolution and peak-to-background ratio, and our study confirms the presence of two magnetic phase transitions. The first of these corresponds to the onset of antiferromagnetic order and the second is interpreted as a 90° reorientation of the basal-plane component of the magnetic moment. In addition, the triangular structure observed at 1.6 °K has been found to undergo considerable modification as the temperature approaches 4.4 °K.

I. INTRODUCTION

Previous neutron-diffraction studies[1–3] of $CsNiCl_3$, which exhibits many of the characteristics of a one-dimensional antiferromagnet, have revealed a magnetic structure in which there are linear antiferromagnetic chains along the hexagonal c axis coupled together in a triangular array with the moments lying in a plane perpendicular to the basal plane. The Néel temperature derived from